2024 IEEE International Conference on Robotics and Automation (ICRA 2024)
May 13-17, 2024. Yokohama, Japan

Thermally-activated Biochemically-sustained Reactor for Soft Fluidic Actuation

Jialun Liu[1], MennaAllah Soliman[1] and Dana D. Damian[1,2]

***Abstract*— Soft robots have shown remarkable distinct capabilities due to their high deformation. Recently increasing attention has been dedicated to developing fully soft robots to exploit their full potential, with a recognition that electronic powering may limit this achievement. Alternative powering sources compatible with soft robots have been identified such as combustion and chemical reactions. A further milestone to such systems would be to increase the controllability and responsiveness of their underlying reactions in order to achieve more complex behaviors for soft robots. In this paper, we present a thermally-activated reactor incorporating a biocompatible hydrogel valve that enables control of the biochemical reaction of sugar and yeast. The biochemical reaction is utilized to generate contained pressure, which in turn powers a fluidic soft actuator. Experiments were conducted to evaluate the response time of the hydrogel valves with three different crosslinker concentrations. Among the tested concentrations, we found that the lowest crosslinker concentration yielded the fastest response time of the valve at an ambient temperature of 50°C. We also evaluated the pressure generation capacity of the reactor, which can reach up to 0.22 bar, and demonstrated the thermo-responsive behavior of the reactor to trigger a biochemical reaction for powering a fluidic soft actuator. This work opens up the possibility to power and control tetherless and fully soft robots.**

I. Introduction

Soft robots have shown remarkable and distinct capabilities due to their high degree of deformation, e.g., life-like growth, computation reduction due to intrinsic compliance to the environment, squeezing through constrained apertures, resilience, and self-healing [1], [2]. There have been notable developments in the area of soft actuators [3], soft sensors [4], and fluidic computation [5]. However, many of these soft devices have relied on bulky and rigid mechanical valves and other classical fluidic components, e.g., pumps [6], compressors [7], [8], pressurized gas tanks [9], or off-the-shelf solenoid valves [10], [11].

Recently, increasing attention has been dedicated to developing fully soft robots to exploit their full potential, with a recognition that electronic powering may limit this achievement. Alternative powering sources compatible with soft robots have been identified, such as combustion and chemical reactions producing gas [12]. For instance, the electrical ignition of a combustible vapor mixture induces a sudden motion of soft actuators [13]. The generation of gas such as carbon dioxide through the neutralization reaction of citric acid and sodium bicarbonate [14] and oxygen through the catalyzed decomposition of hydrogen peroxide [15]–[17] have been studied for powering portable mobile soft robots.

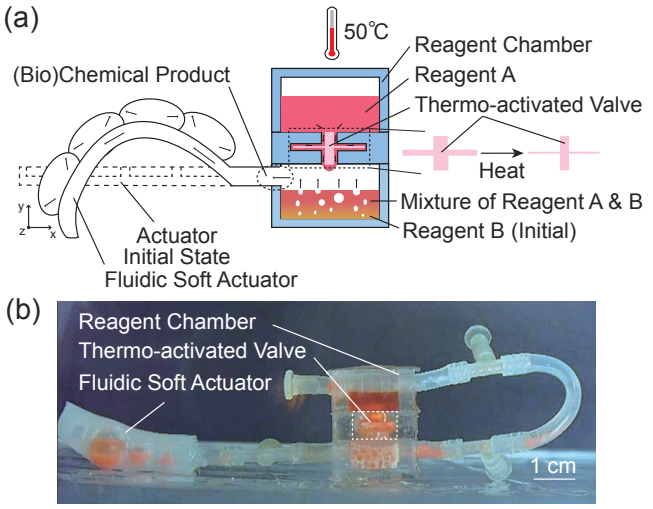

Fig. 1. The thermally-activated reactor. (a) Working principle of the thermally-activated biochemically-sustained reactor for soft fluidic actuation. The hydrogel valve is triggered thermally and shrinks to release reagent from the top reagent chamber to the bottom reagent chamber. The mixing of reagents A and B produces gas as a pressure source for fluidic soft actuators. (b) The photo of the reactor generating pressure to support the bending of a fluidic soft actuator.

A further milestone to such systems would be to increase the controllability and responsiveness of their underlying reactions in order to achieve more complex behaviors for soft robots. Approaches towards this include the introduction of valves and the design of chemical reactions that are triggered by desired stimuli.

Recent work brought advances in remotely triggered soft valves. Examples include magnetic valves using external magnetic sources to control the pressurization of elastomer fluidic actuators [18], [19], Other valve actuation methods have included pneumatic valves which exploit pressure differences in the system, including a valve that can isolate leaking pneumatic chambers in a soft actuator [20], a soft bi-stable valve demonstrating the potential for a soft robot to build a logic control system [21], and force-responsive valve [22]. In the field of microfluidics, work has been carried out towards thermo-responsive valves, exploiting the swelling behaviors of hydrogels to actuate valves. The applications include flow sorters [23] on microfluidic chips, capillary pressure control [24], controllable water transport [25] and on-demand fluid control [26], in order to achieve autonomous flow control for self-regulated microflu-

[1]Automatic Control and Systems Engineering Department, Sheffield Robotics, University of Sheffield, Mappin Street, Sheffield S1 3JD, UK. d.damian@sheffield.ac.uk, jliu222@sheffield.ac.uk [2]Insigneo Institute for *in silico* Medicine, University of Sheffield, UK. This work was supported by an EPSRC DTP Scholarship, an EPSRC DTP ECR Scholarship and the grant EP/X017486/1.

idic systems.

Regarding soft robot alternatives to powering, biochemical reactions are appealing for multiple reasons. Biochemical reactants can show complex responses to a variety of stimuli [27], e.g., temperature, pH, light, and strain. Secondly, they can constitute more human-friendly options making them suitable for medical and in-the-body applications. A soft gripper that detects chemicals in the environment using engineered bacteria was developed in [28]. The investigation of an acoustic field and the resulting 3D motions of microparticles was carried out using yeast in [29]. Yeast is also used as a sensor in [30] by optimizing the operating frequency band of yeast cells cell-on-a-chip based on bio-impedance cytometry for a single cell.

We hypothesize that future soft robots will increasingly rely on natural and organic power sources. Their intelligence will partially be embedded in the physical interaction between these alternative energies and the body materials and mechanisms [31]. Motivated by this vision, in this paper, we present a thermo-responsive biochemical reactor to activate and power a soft fluidic actuator. Temperature is used to trigger both the valve and the biochemical reaction.

The contributions of this work include: 1) design and development of a thermo-activated biochemical reactor; 2) experimental characterization and tuning of a hydrogel valve that activates the reactor; 3) experimental characterization and tuning of the biochemical reaction to optimize gas generation for fluidic powering, and 4) experimental characterization of the pressure generation capability of the reactor, along with a demonstration of the use of the biochemical reactor with a soft actuator.

II. Design, Fabrication and Characterization

Fig. 2 shows the biochemical reactor that could be used for soft robot powering. The reactor enables a mechanical and chemical process, each of which is triggered thermally. The reactor is made of the following main components: 1) two stacked chambers that each store a reactant; 2) a polymer-based smart material valve separating the two chambers which undergoes volume change based on temperature thus blocking or releasing the flow of top chamber reactant in the bottom chamber; and 3) inlets for reactant supply and an outlet for gas release, generated through chemical mixing to power fluidic actuators.

A. Mechanical control principle of the reactor

The top and bottom chambers are used to store reagents, in particular, sugar solution in the top chamber, and activated yeast solution or dry yeast powder in the bottom chamber, for on-board gas generation. The separating layer between the two chambers is equipped with a soft valve made of a thermo-responsive hydrogel (Poly(N-isopropylacrylamide), pNIPAM). This hydrogel has a unique temperature-induced volume change property which can produce macroscopic deformations upon swelling and shrinking. It is hydrophilic when its temperature is below its Lower Critical Solution Temperature (LCST), absorbs water and swells; while it can

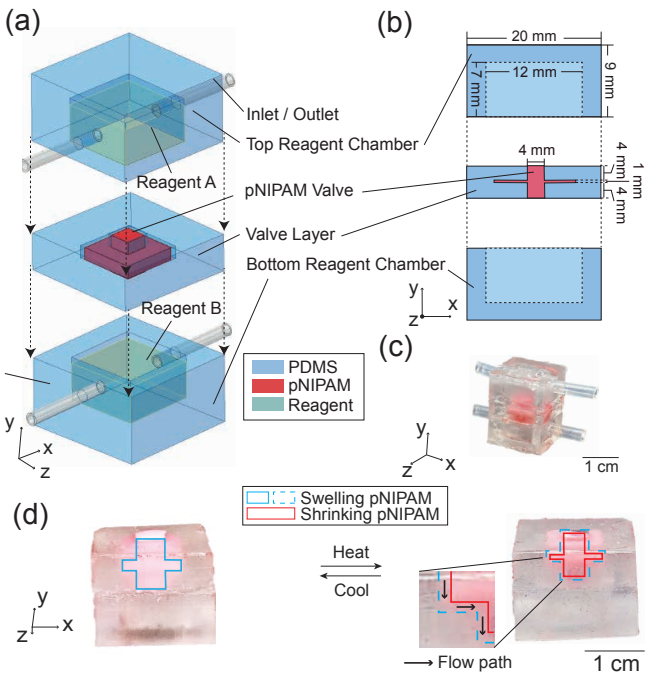

Fig. 2. The thermally-activated reactor design. (a) The schematic design of the reactor. (b) The side view of the schematic design of the reactor with dimensions. (c) The photo of the reactor, the thermo-activated valve is dyed red. (d) Photos of a bottom reagent chamber with a valve above. The valve shrinks when it absorbs heat and swells when it cools down. The dotted lines indicate the volume change.

also be hydrophobic and excrete water and shrink when the temperature is above LCST [32].

As the pNIPAM valve undergoes volume change, it affects the flow of the liquid reagent in the top chamber. At room temperature, the pNIPAM valve is hydrophilic and swollen, preventing the reagent in the top chamber from mixing with the reagent in the bottom chamber. When the temperature of the pNIPAM valve reaches LCST, the pNIPAM shrinks and creates fluid passages around the valve. The reagent from the top flows through the fluid passages due to gravity and mixes with the reagent in the bottom chamber, resulting in the production of gas that escapes into the outlets of the reactor, e.g., soft actuator.

B. Fabrication and Materials

The fabrication of the reactor consists of six steps: moulding of the PDMS reagent chamber and valve layer, preparation of pNIPAM solution, synthesis of pNIPAM valve, cleaning the pNIPAM valve, plasma treatment, and bonding.

1) Fabrication of the reactor chambers: The reagent chamber and the layer separating the chambers (further referred to as chamber-separating layer or valve layer) are made of Polydimethylsiloxane (PDMS). The moulds for PDMS are 3D printed with a stereolithography printer and clear resin (Form 2, Formlabs and clear resin v4, Formlabs). The release agent (Ease Release 200, Mann Release Technologies) is the first sprayed on the surface of printed moulds to help release cured PDMS from the moulds. Four silicon tubes are inserted into the holes for the inlet/outlet on

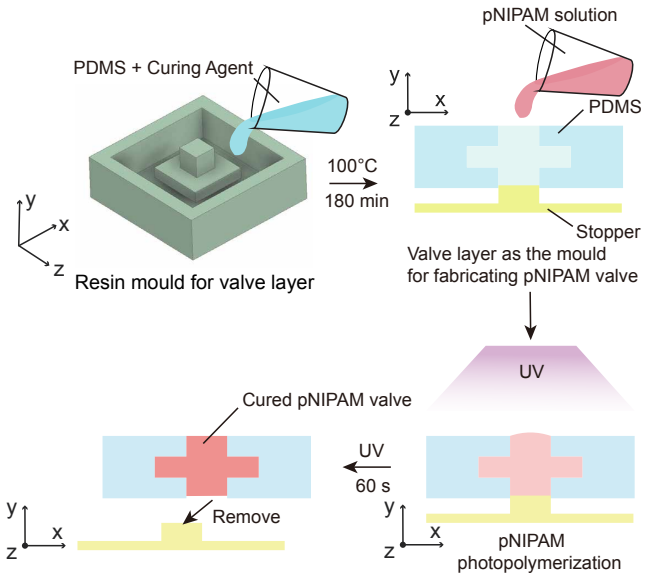

Fig. 3. Synthesis of the pNIPAM valve in the reactor by directly curing the prepared pNIPAM solution in the chamber-separating layer.

two reagent chamber moulds and stay in the moulds during the PDMS curing process. After that, the prepared PDMS prepolymer mixture is poured into the moulds and left at room temperature for 12 hours. The moulds then are heated at 100°C in an oven for 3 hours. The prepolymer mixture is prepared by mixing PDMS prepolymer (Sylgard 184, Dow Chemical Company) with its curing agent in the weight ratio of 10:1 and then degassed in a desiccator with a vacuum pump for 10 minutes. The cured PDMS is removed from the resin moulds to get the reagent chambers and the valve layer.

The two reagent chambers and the valve layer are then treated in a plasma treatment system (Henniker Plasma HPT-200) at 200 W power for 60 s with an atmospheric air flow of 20 sccm. The parameters of the plasma treatment were experimentally found to achieve optimal surface activation. Following plasma treatment, the PDMS chamber walls undergo hydrophilization, enhancing the flow of reagents during gravity-driven mixing.

2) Fabrication of the valve: The pNIPAM prepolymer mixture is prepared by mixing the monomer N-Isopropylacrylamide (NIPAM, Sigma-Aldrich, 1.767M), the crosslinker N,N'-Methylenebisacrylamide (BIS, Sigma-Aldrich, 0.026M - 0.104M) and the photo-initiator Irgacure-2949 (Sigma-Aldrich, 0.018M). After that, the prepolymer mixture is diluted in 50% v/v ethanol solution (Acros Organics) to make pNIPAM solution.

Fig. 3 shows the main steps for synthesis of the pNIPAM valve in the chamber-separating layer. The prepared pNIPAM solution is poured into the plasma-treated chamber-separating layer. A stopper made of acrylic sheets is placed below this layer to prevent pNIPAM solution from leaking. The tip of the stopper has a slightly larger size than the bottom exit of the layer to fully seal the bottom exit. After that, the pNIPAM is cured by placing a UV torch (UTarget-365 nm, UWAVE) above the PDMS layer. The UV with an intensity of 20 W/cm^2 is applied to the pNIPAM solution for 60 s. Then the stopper is removed and the middle layer and the pNIPAM valve are moved to a Petri dish with de-ionized (DI) water for cleaning. The Petri dish is placed on a hot plate until the water temperature reaches 50°C. Then the hot plate is turned off and the water temperature is left to cool to room temperature. The water in the Petri dish is replaced with clean DI water and this cleaning process is repeated once more. This cleaning process helps hydrogel re-hydrate with clean DI water in order to excrete uncured pNIPAM solution in the hydrogel which may affect the thermo-responsive properties of the pNIPAM valve. Subsequently, the two plasma-treated reagent chambers and the valve layer are bonded together to produce the reactor. UV glue (AA 3491, LOCTITE) is also used in this process to ensure the three PDMS parts are bonded well without any leakage.

The valves undergo leakage tests before the full reactor is integrated. During the leakage test, the top reagent chamber, fitted with the valve layer, is filled with the top reactant. This half of the reactor is placed in a Petri dish. We observed if droplets were leaking out of the valve within 24 hours. All the valves used in this paper showed no leakage.

C. Characterization of thermo-responsive valve properties

The properties of the thermo-responsive valve rely on the volume change properties of the pNIPAM hydrogel with temperature. The LCST of pNIPAM hydrogel determines the temperature to trigger the valve. When synthesizing the pNIPAM, the concentration of crosslinker (BIS) affects swelling characteristics. In order to study this, three pNIPAM samples and valves were fabricated with different concentrations of crosslinker. These concentrations are identified as pNIPAM 1 (0.026M BIS), pNIPAM 2 (0.052M BIS) and pNIPAM 3 (0.104M BIS). The synthesized samples have sizes of 8 mm×3 mm×4 mm and were placed in a Petri dish with DI water. The Petri dish was then heated on a hotplate until the water temperature reached 44°C. The size change of the three samples were recorded during this heating process. The swelling ratio is the ratio of the maximum edge length at the given temperature to the maximum edge length at the initial temperature. Fig. 4 (a) shows the measured swelling ratio of three pNIPAM rectangular samples. We can conclude that among the three crosslinker concentrations, an increase in crosslinker concentration tends to result in worse swelling properties, thus giving a slow response speed when pNIPAM is used as a valve. A lower crosslinker concentration creates a lower crosslink density for the polymer network thus leaving more space for the liquid molecules to pass through.

The temperature at which the slope of the volume change curve is the steepest is defined as the LCST. In water, the LCST of the pNIPAM is 32.1°C [33]; however, the LCST of the pNIPAM changes with the pH values of the environment [34], [35]. The bioprocess of yeast and sugar is chosen to be the pressure generation source as the pH of yeast solution, and sugar solution is around 7, which will not change the LCST of the pNIPAM hydrogel dramatically.

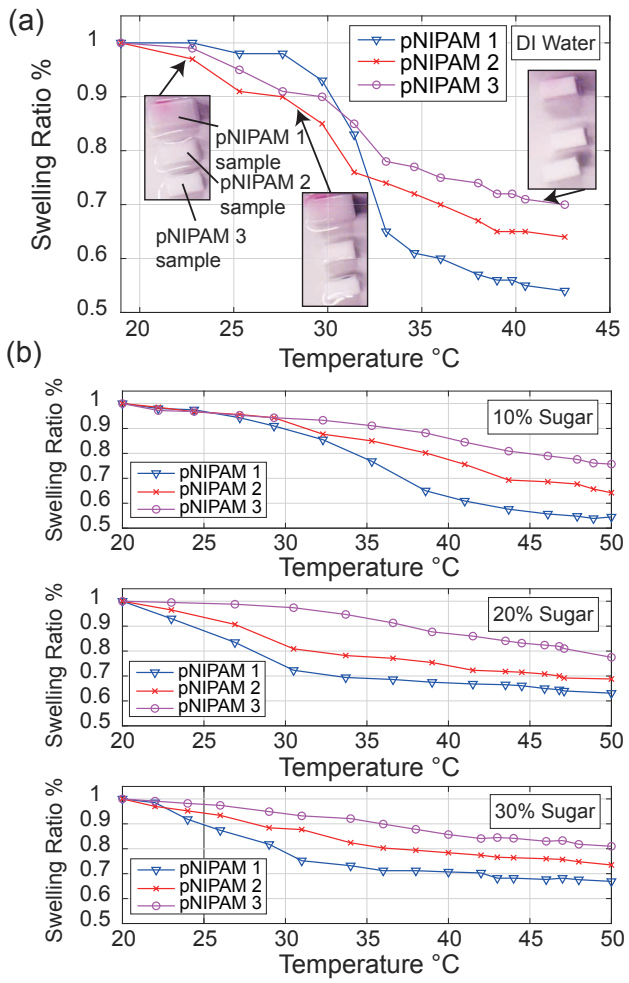

Fig. 4. Volume change behaviors of pNIPAM samples in different liquids at different temperatures. (a) The swelling ratio of three pNIPAM samples with different concentrations of crosslinker in DI water. Photos of pNIPAM samples were taken during the recording process. (b) The swelling ratio of three pNIPAM samples in 10%, 20% or 30% w/w sugar solution.

Similar experiments were conducted to estimate the swelling ratio of three pNIPAM samples in 10% w/w, 20% w/w and 30% w/w sugar solutions. The freshly prepared pNIPAM samples were placed in sugar solutions and heated up until they were fully shrunk. Then the samples were left to cool down until they fully swelled. As a result, the pNIPAM samples had a sugar concentration similar to the solution in which they were bathing, ensuring a consistent swelling response. After that, similar experiments were conducted to measure the swelling ratio. Fig. 4 (b) shows the swelling ratio of three pNIPAM samples in different sugar solutions. It can be seen that the swelling ratios of the three samples are all higher than those in DI water, indicating a decrease in the swelling properties of the hydrogels. This means that the pNIPAM valve will shrink less when the temperature increases, leaving a thinner channel for the reagent from the top chamber to flow to the bottom chamber, resulting in a longer opening time. Also, when the concentrations of sugar solution increase, the swelling properties of the pNIPAM

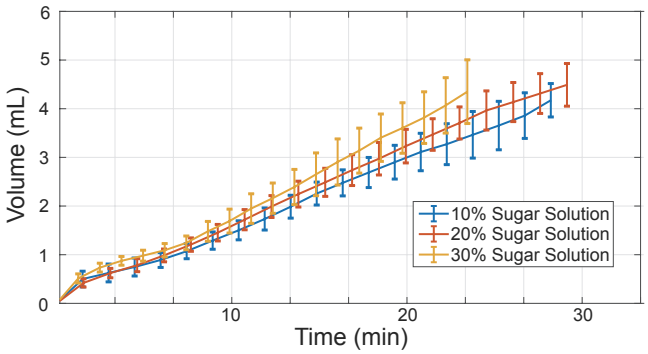

Fig. 5. Volume of CO_2 produced due to the fermentation of three different sugar concentrations with 15% yeast solution over time. The error bars indicate the mean and standard deviation over five trials.

decrease across all three BIS concentrations, indicating a longer valve response time in high concentrations of sugar solution.

D. Characterization of thermo-activated gas generation

The rate of gas generation through the biochemical process of sugar and yeast is affected by sugar concentration and environmental temperature. Experiments were conducted to measure the volume of produced CO_2 gas and the rate of gas generation. Considering the volume of the reagent chamber, equal parts of sugar solution and activated yeast solution were chosen adding up to 1 mL. The yeast used is commercial baking yeast (Saccharomyces cerevisiae, Easy bake yeast, Allinson's). In this experiment, both the yeast concentration and hot bath temperature are fixed, while three sugar concentrations (10%, 20%, and 30%) are tested. A 15% w/w concentration of activated yeast solution is selected as recommended by the literature [36]. For each concentration of sugar solution, five trials are carried out. A measuring cylinder is partially filled with water and placed upside-down in a water tank. 0.5 mL of sugar solution and 0.5 mL of yeast solution are added to a vial with a rubber stopper with tubing. As CO_2 is produced in the vial, it exits through the rubber tubing and displaces the water in the measuring cylinder. The volume of CO_2 is measured by monitoring the volume of the displaced water.

Fig. 5 shows that increasing the sugar concentration increases the gas generation rate; however, comparing 20% and 30% concentration, 20% is more consistent than 30% over the five trials. The stability of 20% was proved by calculating the standard deviation and mean. The standard deviation shows that the variation of 20% is lower than 30%. We found that 20% concentration is most adequate for the reactor as it is more stable and predictable over time.

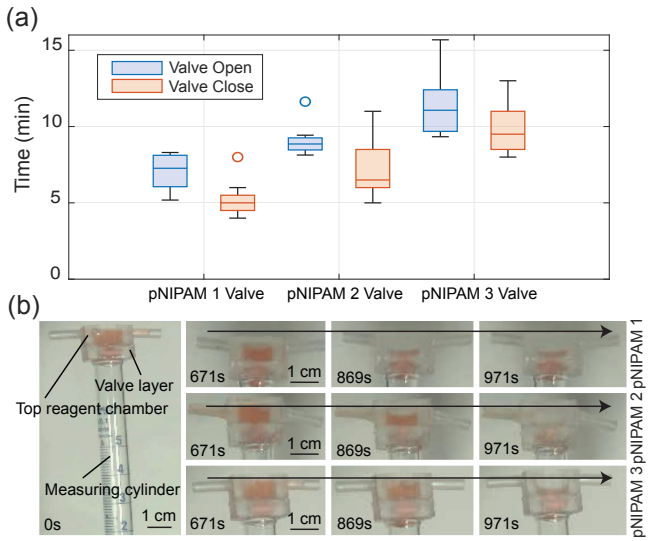

Fig. 6. Thermo-responsive valve characterization. (a) The response time of three different valves with different BIS concentrations. The valve was placed in an environment with 50°C ambient temperature. (b) Snapshots of valves releasing dyed water when being activated thermally. The valves with measuring cylinders were placed in an oven set to 50°C. In some cases, there was a small amount of the liquid left over at the corner of the reagent chamber due to the surface tension of the liquid.

III. Experiments and Results

A. Thermally-activated valving

Experiments evaluated the valve opening/closing times and pressure generation capability. Three valves, made from pNIPAM 1, pNIPAM 2, and pNIPAM 3 solutions in the chamber-separating layer, were fabricated. These valves underwent swelling/shrinking cycles in DI water to remove impurities. The chamber-separating layer was then bonded to a plasma-treated top reagent chamber to create a half reactor. In each experiment, 0.8 mL of red-dyed DI water was syringe-injected into the top reagent chamber with different valves. Valves were placed atop measuring cylinders and exposed to a 50°C oven.

1) Valve opening/closing response time: The valve opening time is when water droplets begin forming at the bottom of the hydrogel valve. After placing the half reactor in the oven and the valve fully shrank and released all liquid, we filled the top chamber with 20°C red-dyed DI water. The chamber was replenished with DI water if the chamber was not full. The valve closing time is defined as the time until no water droplets form at the bottom. Eight experiments were conducted for each valve with varying crosslink densities. Fig. 6 (a) displays recorded opening and closing times. The pNIPAM 1 valve exhibited the fastest response due to significant temperature-induced volume change and lower crosslink density, allowing faster valve action. Fig. 6 (b) shows snapshots of one experiment, illustrating gradual valve opening and liquid release over time. All pNIPAM 1, 2, and 3 valves were functional with no leakage after 30 cycles.

2) Pressure generation capability: Experiments were conducted to measure the pressure generated by the reactor. 0.5 mL of dyed 20% w/w sugar solution were injected in the top reagent chamber while in the bottom chamber, 0.5 mL of 15% w/w activated yeast solution were injected. Sugar and yeast are both dissolved in water, as this allows for thorough mixing of the reactants once the valve is opened. The pNIPAM 1 valve was chosen for its rapid response. After sealing the reactor with stoppers, the top and bottom chambers were connected via a tube and fluidic connectors to equalize pressure in both chambers, ensuring that only gravity drives the liquid to the bottom chamber. A Honeywell 005PGAA5 gauge pressure sensor was connected to the bottom chamber. The setup shown in Fig. 7 (a) was placed in a 50°C preheated oven, where heat from the environment opened the valve, enabling the sugar solution to flow through the fluid passage created by the opened valve, fueling the reaction. The commercial yeast used in experiments can produce some CO2 even without added sugar as it contains a growth medium. As such, control experiments were additionally conducted by removing the sugar supply. Fig. 7 (g) shows the pressure generated among 10 experiments. In 30 minutes, pressure surged up to 0.22 bar. The size of the reactor is directly related to the volume of reagents, which in turn determines the pressure generated.

B. Bioreactor-activated soft actuation

A proof-of-concept demonstration of soft actuation powered by the reactor was prepared. A fluidic soft actuator was connected to one outlet of the bottom chamber. The fluidic soft actuator is fabricated with Ecoflex-50 (Smooth-On, Inc.) following the fabrication method described in [37]. It has a size of 32 mm×6 mm×5 mm and there are 4 inflating chambers with sizes of 3 mm×3 mm×3 mm in the soft actuator. Fig. 7 (b-f) displays the snapshots of this demonstration, while Fig. 7 (h) shows the bending angle over time up to 15.5°. Gas generated in the bottom chamber causes bubbling, pushing liquid back to the top chamber and raising liquid levels. Initially, CO_2 from yeast alone could not bend the actuator. The reactor remained in the oven until gas generation ceased, confirming remote reagent mixing control and actuator pressure production. In the initial 30 minutes, as the pressure increased, the bending angle surged. In the final 30 minutes, as measured in Fig. 7 (g), the pressure stabilized, and the bending angle steadily rose from 11.1° to 15.5°, driven by yeast pushing liquid into the actuator.

IV. Discussion & Conclusion

This paper introduces a thermally-activated reactor incorporating a hydrogel valve that enables control of the biochemical reaction. The biochemical reaction is utilized to generate contained pressure, which in turn powers a soft fluidic actuator. The valve is operated remotely by inducing temperature changes in the reactor. The proposed soft reactor operates in a biochemically-sustained, electronics-free manner, thereby opening up the possibility to power and control untethered and fully soft robots. The hydrogel valve is biocompatible with yeast microorganisms and supports yeast growth within the reactor.

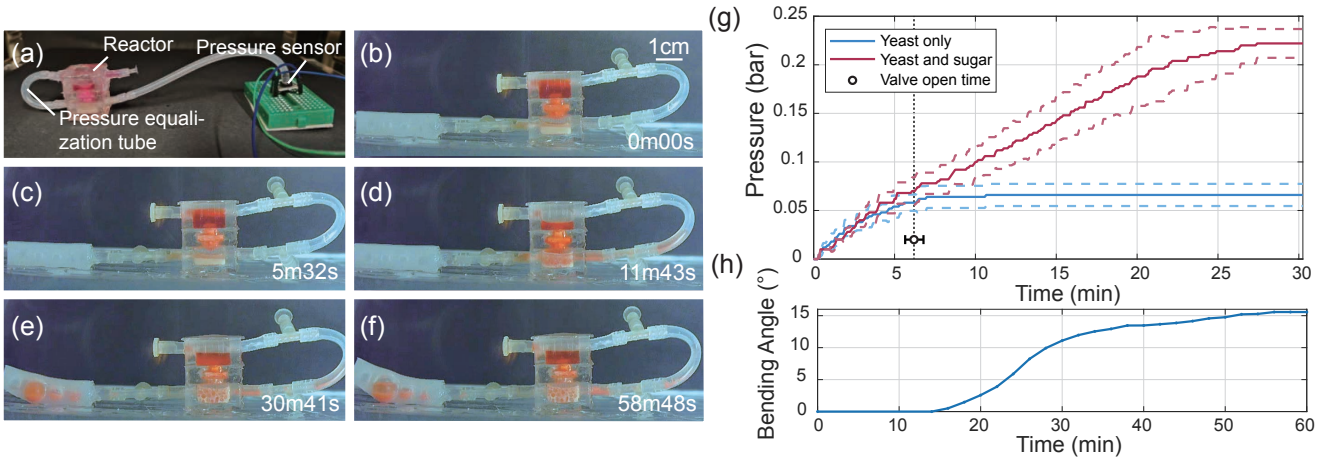

Fig. 7. The proof-of-concept of thermally-activated valving and pressure generation. (a) The experimental setup for measuring the pressure generation capability. (b) Placement of the fueled reactor with a fluidic soft actuator in an oven set to 50°C. (c) Shrinkage of the valve leads the sugar solution to start to flow down and mix with yeast solution in the bottom chamber. (d) Fully shrinkage of the valve lets most of the sugar solution flow down to mix. A small amount of sugar solution is left on the edge of the top chamber due to surface tension. (e, f) The biochemical process of sugar and yeast inflates the soft fluidic actuator. (g) The pressure generated by the reactor is shown in solid curves (mean) and dashed curves (standard deviation) over five trials. The red curve represents pressure generated with sugar and yeast, while the blue curve represents pressure from yeast alone. The black dot with an error bar represents the valve opening time along with its standard deviation across five trials. (h) Bending angle of the soft fluidic actuator against time.

The experiments provide evidence of the reversible functioning of the hydrogel and the one-off performance of the soft actuator. The current reactor prototype does not exploit the reversibility of the valve to regulate the dosage of reactants through mixing or repeated limb motion. To control the pressure within the reactor, the development and installation of an exhaust valve are necessary. Furthermore, it is imperative to replenish the reactant (sugar solution) and eliminate the waste periodically.

In our study, we observed that the reagent chamber size adequately supported the yeast and sugar metabolism. The gas volume rate exhibited satisfactory performance, as demonstrated by the deflection of the miniature actuator inflation. However, further experimentation is required to evaluate the impact of pressure and time on the reactor's performance. To enhance the yeast fermentation process, increasing the yeast quantity or elevating the temperature is possible. Nonetheless, this requires additional controllability over the actuation and deactivation signals. Working with biological components, such as yeast, inevitably introduces behavior variability due to the susceptibility of the organism to room temperature and other airborne bacteria. Furthermore, due to the slow pace of biochemical processes leading to low output power, alternative chemical reactions such as acid-base neutralization reactions can be utilized to achieve significantly faster reaction times while ensuring that the pH remains within a suitable range to avoid damaging the hydrogel. Moreover, the temperature outside of the valve is set to be 50°C in this paper. However, the temperature inside the valve is likely lower than 50°C. The temperature required for the hydrogel to exhibit phase change can be tweaked by modifying the synthesis recipe or grafting the hydrogel with other composites [38]. This makes the triggering temperature controllable in a range of 20-40°C thus providing a potential for medical *in vivo* applications. The biochemical reaction is also affected by temperature, yet this aspect was not within the scope of this work. In the future, we will investigate the effect of temperature on both the valve mechanics and biochemical reactions, seeking the possibility to differentiate their control and thus achieve greater controllability. Our future research endeavors encompass the miniaturization of the reactor to facilitate the construction of a fully mobile soft robot, the development of a replenishment and waste elimination mechanism, enabling remote hydrogel valve triggering using magnetic induction [39], and exploring the biomedical applications for this reactor.

V. Acknowledgement

We acknowledge the valuable contributions of Shuhei Miyashita, Quentin Lahondes and Marco Pontin. We thank Joanna Jones, Frederick Forbes and Kaan Esendag for reviewing the manuscript. We appreciate the feedback from the members of Sheffield Biomedical Robotics Lab and Sheffield Microrobotics Lab.

References

[1] E. W. Hawkes, L. H. Blumenschein, J. D. Greer, and A. M. Okamura, "A soft robot that navigates its environment through growth," *Science Robotics*, vol. 2, no. 8, p. eaan3028, 2017.

[2] D. Rus and M. T. Tolley, "Design, fabrication and control of soft robots," *Nature*, vol. 521, no. 7553, pp. 467–475, 2015.

[3] J. Hughes, U. Culha, F. Giardina, F. Guenther, A. Rosendo, and F. Iida, "Soft manipulators and grippers: a review," *Frontiers in Robotics and AI*, vol. 3, p. 69, 2016.

[4] M. Cianchetti, C. Laschi, A. Menciassi, and P. Dario, "Biomedical applications of soft robotics," *Nature Reviews Materials*, vol. 3, no. 6, pp. 143–153, 2018.

[5] Y. Xu, C. Huang, D. Li, J. Liu, S. Fu, X. Wu, and T. Xu, "Cooperative control strategy of magnetic microrobots in bifurcated microfluidic channels," *IEEE Robotics and Automation Letters*, vol. 8, no. 4, pp. 1889–1896, 2023.

[6] Q. Tan, Y. Chen, J. Liu, K. Zou, J. Yi, S. Liu, and Z. Wang, "Underwater crawling robot with hydraulic soft actuators," *Frontiers in Robotics and AI*, vol. 8, 2021.

[7] K. Xu and N. O. Pérez-Arancibia, "Electronics-free logic circuits for localized feedback control of multi-actuator soft robots," *IEEE Robotics and Automation Letters*, vol. 5, no. 3, pp. 3990–3997, 2020.

[8] M. T. Tolley, R. F. Shepherd, M. Karpelson, N. W. Bartlett, K. C. Galloway, M. Wehner, R. Nunes, G. M. Whitesides, and R. J. Wood, "An untethered jumping soft robot," in *2014 IEEE/RSJ International Conference on Intelligent Robots and Systems*, pp. 561–566, 2014.

[9] M. Wehner, M. T. Tolley, Y. Mengüç, Y.-L. Park, A. Mozeika, Y. Ding, C. Onal, R. F. Shepherd, G. M. Whitesides, and R. J. Wood, "Pneumatic energy sources for autonomous and wearable soft robotics," *Soft robotics*, vol. 1, no. 4, pp. 263–274, 2014.

[10] J. W. Booth, J. C. Case, E. L. White, D. S. Shah, and R. Kramer-Bottiglio, "An addressable pneumatic regulator for distributed control of soft robots," in *2018 IEEE International Conference on Soft Robotics (RoboSoft)*, pp. 25–30, 2018.

[11] G. Gerboni, T. Ranzani, A. Diodato, G. Ciuti, M. Cianchetti, and A. Menciassi, "Modular soft mechatronic manipulator for minimally invasive surgery (mis): overall architecture and development of a fully integrated soft module," *Meccanica*, vol. 50, pp. 2865–2878, 2015.

[12] M. Adami and A. Seibel, "On-board pneumatic pressure generation methods for soft robotics applications," in *Actuators*, vol. 8, p. 2, 2018.

[13] R. F. Shepherd, A. A. Stokes, J. Freake, J. Barber, P. W. Snyder, A. D. Mazzeo, L. Cademartiri, S. A. Morin, and G. M. Whitesides, "Using explosions to power a soft robot," *Angewandte Chemie International Edition*, vol. 52, no. 10, pp. 2892–2896, 2013.

[14] M. Okui, Y. Nagura, S. Iikawa, Y. Yamada, and T. Nakamura, "A pneumatic power source using a sodium bicarbonate and citric acid reaction with pressure booster for use in mobile devices," in *2017 IEEE/RSJ International Conference on Intelligent Robots and Systems (IROS)*, pp. 1040–1045, 2017.

[15] K.-R. Kim, Y. J. Shin, K.-S. Kim, and S. Kim, "Application of chemical reaction based pneumatic power generator to robot finger," in *2013 IEEE/RSJ International Conference on Intelligent Robots and Systems*, pp. 4906–4911, 2013.

[16] M. Wehner, R. L. Truby, D. J. Fitzgerald, B. Mosadegh, G. M. Whitesides, J. A. Lewis, and R. J. Wood, "An integrated design and fabrication strategy for entirely soft, autonomous robots," *Nature*, vol. 536, no. 7617, pp. 451–455, 2016.

[17] C. D. Onal, X. Chen, G. M. Whitesides, and D. Rus, "Soft mobile robots with on-board chemical pressure generation," in *Robotics Research: The 15th International Symposium ISRR*, pp. 525–540, 2017.

[18] Y. Miyaki and H. Tsukagoshi, "Self-excited vibration valve that induces traveling waves in pneumatic soft mobile robots," *IEEE Robotics and Automation Letters*, vol. 5, no. 3, pp. 4133–4139, 2020.

[19] A. D. Marchese, C. D. Onal, and D. Rus, "Soft robot actuators using energy-efficient valves controlled by electropermanent magnets," in *2011 IEEE/RSJ International Conference on Intelligent Robots and Systems*, pp. 756–761, 2011.

[20] M. Pontin, S. Miyashita, and D. D. Damian, "Development and characterization of a soft valve for automatic fault isolation in inflatable soft robots," in *2022 IEEE 5th International Conference on Soft Robotics (RoboSoft)*, pp. 62–67, 2022.

[21] P. Rothemund, A. Ainla, L. Belding, D. J. Preston, S. Kurihara, Z. Suo, and G. M. Whitesides, "A soft, bistable valve for autonomous control of soft actuators," *Science Robotics*, vol. 3, no. 16, p. eaar7986, 2018.

[22] A. J. Partridge and A. T. Conn, "Passive, reflex response units for reactive soft robotic systems," *IEEE Robotics and Automation Letters*, vol. 5, no. 3, pp. 4014–4020, 2020.

[23] D. J. Beebe, J. S. Moore, J. M. Bauer, Q. Yu, R. H. Liu, C. Devadoss, and B.-H. Jo, "Functional hydrogel structures for autonomous flow control inside microfluidic channels," *Nature*, vol. 404, no. 6778, pp. 588–590, 2000.

[24] S. Wang, X. Zhang, C. Ma, S. Yan, D. Inglis, and S. Feng, "A review of capillary pressure control valves in microfluidics," *Biosensors*, vol. 11, no. 10, p. 405, 2021.

[25] H. Geng, K. Zhou, J. Zhou, H. Ma, C. Lv, C. Li, Z. Xu, and L. Qu, "Sunlight-driven water transport via a reconfigurable pump," *Angewandte Chemie*, vol. 130, no. 47, pp. 15661–15666, 2018.

[26] S. Sugiura, A. Szilágyi, K. Sumaru, K. Hattori, T. Takagi, G. Filipcsei, M. Zrínyi, and T. Kanamori, "On-demand microfluidic control by micropatterned light irradiation of a photoresponsive hydrogel sheet," *Lab Chip*, vol. 9, pp. 196–198, 2009.

[27] S. Mantha, S. Pillai, P. Khayambashi, A. Upadhyay, Y. Zhang, O. Tao, H. M. Pham, and S. D. Tran, "Smart hydrogels in tissue engineering and regenerative medicine," *Materials*, vol. 12, no. 20, p. 3323, 2019.

[28] K. B. Justus, T. Hellebrekers, D. D. Lewis, A. Wood, C. Ingham, C. Majidi, P. R. LeDuc, and C. Tan, "A biosensing soft robot: Autonomous parsing of chemical signals through integrated organic and inorganic interfaces," *Science Robotics*, vol. 4, no. 31, p. eaax0765, 2019.

[29] X. Tao, T. Dai Nguyen, H. Jin, R. Tao, J. Luo, X. Yang, H. Torun, J. Zhou, S. Huang, L. Shi, *et al.*, "3d patterning/manipulating microparticles and yeast cells using zno/si thin film surface acoustic waves," *Sensors and Actuators B: Chemical*, vol. 299, p. 126991, 2019.

[30] J. Claudel, A. L. Alves De Araujo, M. Nadi, and D. Kourtiche, "Lab-on-a-chip device for yeast cell characterization in low-conductivity media combining cytometry and bio-impedance," *Sensors*, vol. 19, no. 15, p. 3366, 2019.

[31] M. Filippi, O. Yasa, R. D. Kamm, R. Raman, and R. K. Katzschmann, "Will microfluidics enable functionally integrated biohybrid robots?," *Proceedings of the National Academy of Sciences*, vol. 119, no. 35, p. e2200741119, 2022.

[32] H. Schild, "Poly(n-isopropylacrylamide): experiment, theory and application," *Progress in Polymer Science*, vol. 17, no. 2, pp. 163–249, 1992.

[33] Q. Lahondes and S. Miyashita, "Temperature driven soft reversible self-folding origami string," in *2022 IEEE 5th International Conference on Soft Robotics (RoboSoft)*, pp. 589–594, 2022.

[34] S. Chen, L. Jiang, and Y. Dan, "Thermal response and morphology of poly(n-isopropylacrylamide) microgels based on different initiators and different ph environments," *Journal of Macromolecular Science, Part B*, vol. 51, no. 6, pp. 1057–1068, 2012.

[35] J. Ma, B. Fan, B. Liang, and J. Xu, "Synthesis and characterization of poly(n-isopropylacrylamide)/poly(acrylic acid) semi-ipn nanocomposite microgels," *Journal of Colloid and Interface Science*, vol. 341, no. 1, pp. 88–93, 2010.

[36] D. H. Maloney and J. J. Foy, "Yeast fermentations," in *Handbook of dough fermentations*, pp. 67–86, CRC Press, 2003.

[37] B. Mosadegh, P. Polygerinos, C. Keplinger, S. Wennstedt, R. F. Shepherd, U. Gupta, J. Shim, K. Bertoldi, C. J. Walsh, and G. M. Whitesides, "Pneumatic networks for soft robotics that actuate rapidly," *Advanced Functional Materials*, vol. 24, no. 15, pp. 2163–2170, 2014.

[38] S. Huang, J. Shen, N. Li, and M. Ye, "Dual ph- and temperature-responsive hydrogels with extraordinary swelling/deswelling behavior and enhanced mechanical performances," *Journal of Applied Polymer Science*, vol. 132, no. 9, 2015.

[39] J. Liu, X. Chen, Q. Lahondes, K. Esendag, D. Damian, and S. Miyashita, "Origami robot self-folding by magnetic induction," in *2022 IEEE/RSJ International Conference on Intelligent Robots and Systems (IROS)*, pp. 2519–2525, 2022.